Journal of
Applied Crystallography

ISSN 0021-8898

Received 16 August 2006
Accepted 5 January 2007

Effects of side-chain length on the magnetic response of discotic metallomesogens

Ji-Hwan Lee,[a] Hyo-Sik Kim,[a] Brian D. Pate[b] and Sung-Min Choi[a]*

[a]Department of Nuclear and Quantum Engineering, Korea Advanced Institute of Science and Technology, Daejeon, 305-701, Republic of Korea, and [b]Department of Materials Science and Engineering, Institute for Soldier Nanotechnologies, Massachusetts Institute of Technology, Cambridge, MA 02139, USA. Correspondence e-mail: sungmin@kaist.ac.kr

The magnetic responses of columnar superstructures of discotic metallomesogens with different alkyl side-chain lengths, cobalt octa(*n*-alkylthio)porphyrazine (CoS*x*, where *x* is the peripheral *n*-alkyl chain length, $x = 10, 12, 14$), have been investigated by small-angle neutron scattering (SANS). CoS*x* ($x = 10, 12, 14$) were heated to their isotropic phases and cooled down to their columnar mesophases under various external magnetic fields (0.2–1.1 T) and the orientational orderings of the columnar mesophases were measured by SANS. The SANS patterns showed clear anisotropies indicating the alignment of columnar domains with their columnar directors perpendicular to the applied magnetic field. The annularly averaged SANS data, $I(\Phi)$, of CoS*x* ($x = 10, 12, 14$) under various magnetic field strengths were fitted with Lorentzian functions. The full width at half maximum (FWHM) of the $I(\Phi)$ of CoS10 and CoS12 rapidly decreases with increasing applied magnetic field and then saturates to about 42° at ~0.5 T and 50° at ~0.6 T, respectively. In the case of CoS14, however, the diffraction anisotropy was very weak even at field strengths as high as 1.13 T and the FWHM was very broad, *ca*. 120°. The dramatic decrease of magnetic field sensitivity of CoS14 may be attributed to the entropy increase with the side-chain length.

1. Introduction

Columnar discotic liquid crystals (DLCs), which consist of disc-like molecules with an aromatic core and peripheral side chains, offer one-dimensional charge transport along the overlapping π orbitals of the stacked aromatic cores (Schouten *et al.*, 1991; Adam *et al.*, 1993; Simmerer *et al.*, 1996). Therefore, DLCs have been investigated for opto-electronic applications such as photovoltaic cells (Schmidt-Mende *et al.*, 2001; Samori *et al.*, 2004), field-effect transistors (Van de Craats *et al.*, 2003; Jäckel *et al.*, 2004; Pisula *et al.*, 2005) and organic light-emitting diodes (Seguy *et al.*, 2000; O'Neill & Kelly, 2003). However, for practical applications, long-range unidirectional alignment of the columnar DLC structure is crucial.

Various alignment techniques for columnar discotic liquid crystals have been investigated so far, such as mechanical stretching (Van Winkle & Clark, 1982), Langmuir–Blodgett deposition (Josefowicz *et al.*, 1993; Smolenyak *et al.*, 1999; Laursen *et al.*, 2004) and utilization of pre-aligned layers (Zimmermann *et al.*, 2002; Bunk *et al.*, 2003; Van de Craats *et al.*, 2003). Magnetic alignment techniques, however, have been reported as an efficient method to obtain highly oriented columnar structures over a bulk length scale (Pate *et al.*, 2002; Shklyarevskiy *et al.*, 2005; Lee, Choi *et al.*, 2006; Lee, Kim *et al.*, 2006). The free energy of magnetic alignment for DLC systems can be expressed as $\Delta G_{\rm align} = -(1/2)\Delta\chi(\mathbf{H}\cdot\mathbf{n})^2$ where $\Delta\chi$ is the anisotropy of magnetic susceptibility, $\mathbf{H}$ is an applied magnetic field, and $\mathbf{n}$ is the columnar director. Due to the large negative diamagnetic anisotropy of the aromatic core ($\Delta\chi < 0$) of most discotic mesogens, the columnar directors align perpendicular to the applied magnetic field (Dekker, 1987; Boden *et al.*, 1993).

Recently, Pate *et al.* (2002) investigated the magnetic response of a series of octa(*n*-alkylthio)metalloporphyrazine liquid crystals with different metal centers (*M*S10, *M* = Co, Ni, Cu, and Zn, *n*-alkyl = $C_{10}H_{21}$, Fig. 1) which exhibit hexagonal columnar mesophases. Small-angle neutron scattering (SANS) measurements of *M*S10 (*M* = Co, Ni, and Zn) revealed that the columnar directors orient perpendicular to the applied static magnetic field as low as 0.5 T when the samples were cooled from the isotropic phase. On the other hand,

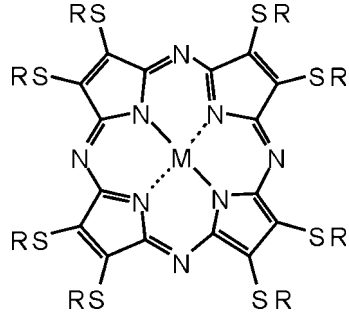

Figure 1
Chemical structure of the discotic liquid crystals octa(*n*-alkylthio)metalloporphyrazine.

Table 1
Configuration of SANS instruments.

Instrument	Wavelength (λ, Å)/ FWHM (Δλ/λ)	Source/sample aperture diameter (mm)	Source-to-sample/ sample-to-detector distance (m)	Detector offset (cm)/ tilt angle (°)
8 m SANS at HANARO	4.31/0.10	32/8	4.5/2.0	15/2.5
NG3 30 m SANS at NCNR	4.45/0.167	50.8/9.5	5.47/1.87	20/none

CuS10 exhibited no preferred alignment at fields as high as 1.02 T. These differences were attributed to the competition of the diamagnetic moments of the aromatic cores and the paramagnetic moments of metal centers. In the case of CoS10, which showed the highest magnetic response among the *M*S10 compounds, both moments work constructively, enhancing magnetic alignment.

In our recent study, it was shown that the uniaxial alignment of the columnar superstructure of CoS12 over the centimetre length scale can be achieved by spinning samples under a static magnetic field (Lee, Choi *et al.*, 2006). When the samples were continuously spun during cooling from the isotropic phase to the columnar mesophase under a static magnetic field (1.0 T), CoS12 was observed to form uniaxially aligned columnar superstructures with the columnar domain directors being parallel to the rotation axis, which was normal to the external field. The optimal rotation speed for the alignment was found to be as low as 5–10 r.p.m., where the full width at half maximum (FWHM) of the domain director distribution is minimized.

Since the alignment technique using an external magnetic field requires cooling from the isotropic phase to the columnar liquid crystalline phase, the isotropic to liquid crystalline (LC) phase transition temperature should be located in the range of temperature which allows practical thermal processing without degrading the molecules. Also the applied magnetic field strength needs to be reasonably low to facilitate the alignment process. The phase behavior of the DLCs is governed by the enthalpic gain from the crystal-like packing of discs within a column and the entropic contribution of side-chain mobility (Simpson *et al.*, 2004). While the isotropic to LC phase transition temperature increases with the size of the aromatic core, it decreases with the side-chain length. Therefore, to optimize the degree of magnetic alignment of DLCs, the size of the aromatic core and the length of the side chain of DLCs should be properly selected.

In this study, we investigated the effects of the alkyl side-chain length on the magnetic response of CoS*x* (x = 10, 12, 14) with different side-chain lengths, which were characterized by SANS measurements. To our knowledge, this is the first study on the effects of side-chain length on the magnetic alignment of the columnar DLCs using SANS.

2. Experimental

2.1. Materials

Cobalt 2,3,7,8,12,13,17,18-octa(*n*-alkylthio)porphyrazine (*n*-alkyl = C_xH_{2x+1}, x = 10) was synthesized in-house and CoS12 and CoS14 were purchased from INNO BioSystem, which utilizes an analog of the synthetic procedure which is described elsewhere (Lelj *et al.*, 1992; Doppelt & Huille, 1990).

2.2. Methods

Differential scanning calorimetry (DSC) measurements were performed in a nitrogen atmosphere using a Dupont 2010 DSC instrument at a scanning rate of 10 K min^{-1}. The instrument was calibrated with an indium standard.

Thermogravimetric analysis (TGA) measurements were performed in a nitrogen atmosphere using a Dupont TGA-Q500 instrument at a scanning rate of 5 K min^{-1}. Samples were heated to 773 K.

Polarized optical microscopy (POM) measurements were performed using an Olympus BX51 polarized optical microscope. Sample temperatures were controlled using a Linkam LTS 350 hot stage at a scanning rate of 1 K min^{-1}.

SANS measurements were performed using the 8 m SANS instrument at the High-flux Advanced Neutron Application Reactor (HANARO) of the Korea Atomic Energy Research Institute in Daejeon, Korea, and the 30 m instrument (NG3) at the NIST Center for Neutron Research (NCNR) in Gaithersburg, MD, USA. The instrument configurations employed at HANARO and NCNR are summarized in the Table 1. The scattering intensities were measured using a two-dimensional detector as a function of scattering vector **q**, $|\mathbf{q}| = q = (4\pi/\lambda)\sin\theta$ where λ is the wavelength and 2θ is the scattering angle. The q ranges used in this study were 0.020–0.42 Å^{-1} (HANARO) and 0.025–0.48 Å^{-1} (NCNR). Scattering from the samples was corrected for background and empty cell scattering. All the collected data sets were circularly or annularly averaged using data reduction software provided by the NCNR.

Each sample as its isotropic phase was loaded into a disc-shaped cell (1.6 cm in diameter and 0.1 cm in thickness or beam path length) enclosed by two quartz disc windows. The sample was measured as loaded with the incident neutron beam direction, **N**, perpendicular to the direction of the applied magnetic field **H**. The temperature-controlled holder which contains the sample cell was placed between the poles of an electromagnet (HV7H for the measurements at HANARO and HV7W for the measurements at NCNR, Walker LDJ Scientific Inc.) with a 62–66 mm pole gap, providing field strengths of up to 1.1 T.

3. Results and discussions

3.1. Phase behavior of CoS*x*

The phase transition temperatures of CoS*x* (x = 10, 12, 14) were identified from DSC, POM, and SANS measurements during heating and cooling. The transition temperatures measured using DSC instruments with a scanning rate of 10 K min^{-1} are summarized in Table 2. The transition temperatures determined from the different techniques were consistent within a few K. They are also consistent with previous studies (Lelj *et al.*, 1992). Some degree of fluidity in the LC phase of a discotic mesogen at room temperature leads to self-healing ability after columnar formation (Simpson *et al.*, 2004). As the side-chain length increases, the transition temperature from the isotropic phase to the LC phase decreases and the temperature range of the LC phase becomes narrower. The focal conic texture of a typical hexagonal columnar LC phase of CoS10 is depicted in Fig. 2. This texture was observed for all CoS*x* (x = 10, 12, 14) in their mesophases. The degradation temperatures of CoS*x* (x = 10, 12, 14)

Table 2
Phase transition temperatures and intercolumnar distances of CoSx in their hexagonal columnar LC phases (x = 10, 12, 14).

T_m: phase transition temperature from the solid to the liquid crystalline phase (LC). T_i: phase transition temperature from the LC to the isotropic phase. T_d: degradation temperature.

x	T_m (K) heating/cooling	a (Å)	T_i (K) heating/cooling	T_d (K)
10	337/—†	24.9	451/438	502
12	353/324	27.9	400/389	523
14	350/314	29.8	397/371	506

† No phase transition was observed until the sample was cooled down to 308 K.

identified from TGA measurements are summarized in Table 2. Here, the degradation temperatures were determined as the temperature at which the sample mass was reduced by 2%.

The SANS intensities of CoS14 that represent the isotropic, LC, and crystalline phases, respectively, are shown in Fig. 3. The sharp peak in the LC phase is consistent with the high degree of ordering associated with the hexagonal columnar LC lattice. The intercolumnar distances a [$a = d/\cos 30^\circ$ for a hexagonal system, where d is the lattice spacing of the (100) plane] of CoSx (x = 10, 12, 14) were determined from the peak positions of the LC phases and are summarized in Table 2. As the side-chain length becomes longer, the intercolumnar spacing a in the hexagonal columnar mesophase increases accordingly.

3.2. Magnetic response of CoSx

In order to compare the magnetic response of CoSx derivatives with different side-chain lengths, SANS measurements of the CoSx (x = 10, 12, 14) derivatives were performed under a series of applied magnetic field strengths. Each sample was first heated to a temperature well into its liquid phase (CoS10: 473 K; CoS12: 473 K; and CoS14: 413 K; the temperatures are lower than the degradation temperatures that were determined by TGA measurements) where the diffraction peak was broad and isotropic. The applied external magnetic field was then adjusted to the desired strength, and the sample was cooled down to a fixed temperature well into its columnar LC phase (CoS10: 353 K; CoS12: 363 K; and CoS14: 343 K). The cooling rate was approximately 5 K min^{-1}. After allowing some equilibration time, SANS measurements were performed. These steps were repeated for different field strengths. The two-dimensional SANS data of CoS10, measured in the absence of an external magnetic field, exhibited a sharp peak with isotropic distribution (Fig. 4, left). This indicates that the bulk DLC samples comprise ordered columnar domains which have randomly oriented domain directors. On the other hand, the two-dimensional SANS data measured in the presence of an applied magnetic field (1.0 T) were distinctly anisotropic with the maximum intensity along the field direction, as shown in Fig. 4 (right). This clearly indicates that the domain directors, which are parallel to the columnar directors, are oriented perpendicular to the applied field. While similar behavior

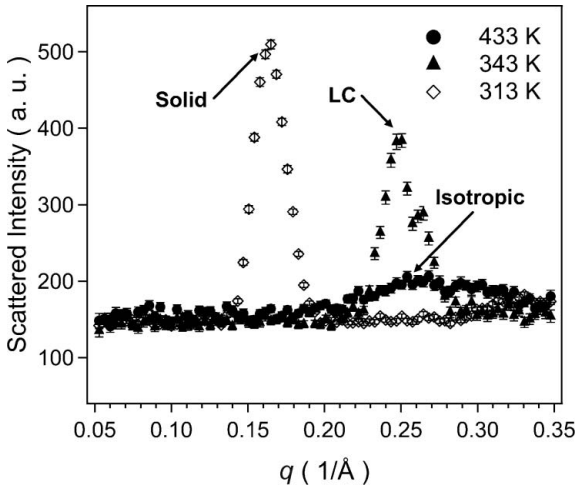

Figure 3
SANS intensities of CoS14 in different phases. The measurements were performed upon cooling. (a.u.: arbitrary units.)

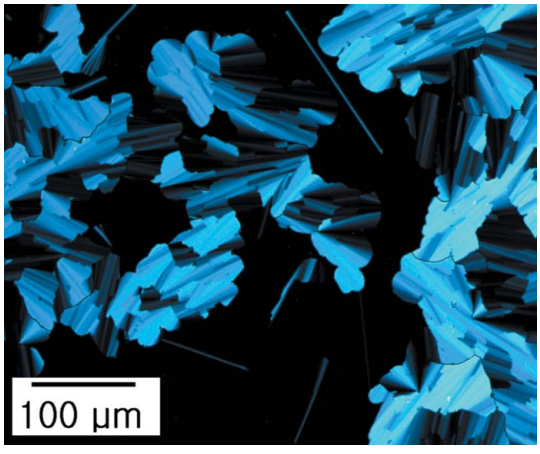

Figure 2
The optical texture of CoS10 at 353 K under crossed polarizers, in its columnar hexagonal columnar LC phase, was measured upon cooling at a rate of 1 K min^{-1}.

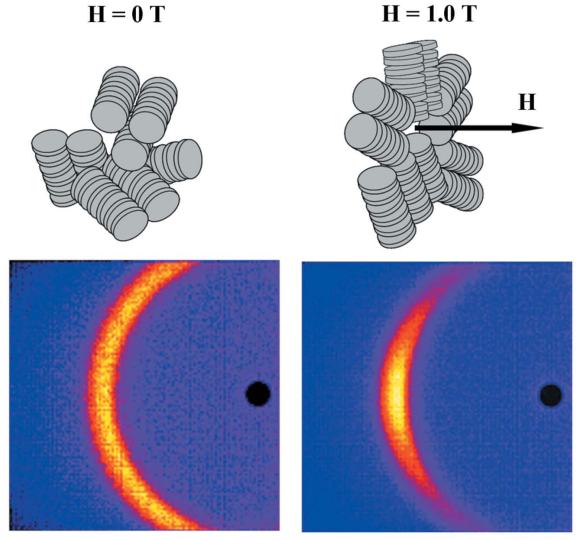

Figure 4
Two-dimensional SANS patterns for CoS10 in the LC phase with and without an applied magnetic field. The samples were cooled from the isotropic phase down to the LC phase (left) in the absence and (right) in the presence of the applied magnetic field of 1.0 T. For the pattern on the right, **N** ⊥ **H**. The sketches show the induced orientations of the domain directors.

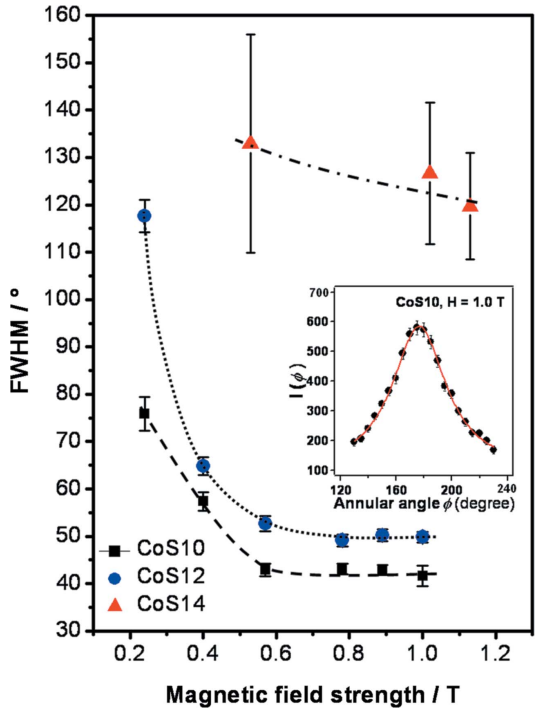

Figure 5
FWHMs of the annularly averaged SANS data of CoSx (x = 10, 12, 14) as a function of the applied magnetic field strength. The inset shows a Lorentzian fit for the SANS data of CoS10 cooled from its isotropic phase under **H** = 1.0 T. The measurements were performed at 353 K for CoS10, 363 K for CoS12, and 343 K for CoS14, at which the samples are in their columnar liquid crystalline phases.

was observed for CoS12, the scattering pattern of CoS14 was much less anisotropic.

The two-dimensional SANS data were annularly averaged at q = 0.285 Å^{-1} for CoS10, q = 0.269 Å^{-1} for CoS12 and q = 0.243 Å^{-1} for CoS14, respectively. The annularly averaged SANS data, $I(\Phi)$, of CoSx (x = 10, 12, 14) under various magnetic field strengths were fitted with Lorentzian functions (inset of Fig. 5). The FWHMs of $I(\phi)$ as a function of the applied magnetic field strength are shown in Fig. 5. The FWHMs of $I(\phi)$ for CoS10 and CoS12 decrease rapidly with the applied magnetic field strength and then saturate to about 42° at ~0.5 T and 50° at ~0.6 T. In the case of CoS14, however, the FWHM of $I(\phi)$ is very broad, *ca*. 120°, even at field strengths as high as 1.13 T, and its dependence on the field strength is rather small. These results indicate that the saturating magnetic field strength for the alignment increases with the side-chain length x, which may be attributed to the entropy increase with the side-chain length. It should be also noted that the saturating magnetic fields for the alignments of CoS10 and CoS12 are much lower than those for other DLCs (Boden *et al.*, 1993; Eichhorn *et al.*, 2003). This can be attributed to the constructive effects of the diamagnetic moments of the aromatic core and the paramagnetic moments of the central cobalt atom of CoS10 and CoS12 (Pate *et al.*, 2002; Lee, Choi *et al.*, 2006).

4. Conclusions

The effects of side-chain length on the magnetic alignments of columnar discotic metallomesogens, cobalt octa(*n*-alkylthio)porphyrazine (CoSx, x = 10, 12, 14), have been investigated by SANS. The DSC, POM, and SANS measurements showed that as the side-chain length increased, the transition temperature from the columnar LC phase to the isotropic phase decreases. The SANS measurements, which were performed after the samples were cooled down from the isotropic phase to the columnar LC phase under various external magnetic fields, showed clear anisotropies indicating the alignments of columnar domains with their columnar directors perpendicular to the applied magnetic field. The FWHM of the annularly averaged SANS data decreases with applied magnetic field strength and then saturates to about 42° at ~0.5 T (CoS10) and 50° at ~0.6 T (CoS12), respectively. In the case of CoS14, however, the FWHM was very broad, *ca*. 120°, even at 1.13 T. The increase of threshold magnetic field strength with the side-chain length may be attributed to the entropy increases with the side-chain length. In summary, with the longer side-chain length, the magnetic alignment process can occur at lower temperature, which facilitates the alignment process and reduces the decomposition of molecules, but the magnetic field strength required for the alignment becomes higher. Therefore, to optimize the magnetic alignments of discotic metallomesogens, the side-chain length should be properly selected.

This work was supported by the program of the Basic Atomic Energy Research Institute (BAERI) and the cold neutron research facility development project which are part of the Nuclear R&D Programs funded by the Ministry of Science & Technology (MOST) of Korea. H.-S. Kim is partially supported by the Brain Korea 21 program. We thank the HANARO at KAERI for SANS beamtime support. Part of the SANS measurements utilized the NIST facilities supported in part by the National Science Foundation under DMR-9986442.

References

Adam, D., Closs, D., Frey, T., Funhoff, D., Haarer, D., Ringsdorf, H., Schuhmacher, P. & Siemensmeyer, K. (1993). *Phys. Rev. Lett.* **70**, 457–460.
Boden, N., Bushby, R. J. & Clements, J. (1993). *J. Chem. Phys.* **98**, 5920–5931.
Bunk, O., Nielsen, M. M., Sølling, T. I., Van de Craats, A. M. & Stutzmann, N. (2003). *J. Am. Chem. Soc.* **125**, 2252–2258.
Dekker, A. J. (1987). *Can. J. Phys.* **65**, 1185–1193.
Doppelt, P. & Huille, S. (1990). *New J. Chem.* **14**, 607–609.
Eichhorn, S. H., Adavelli, A., Li, H. S. & Fox, N. (2003). *Mol. Cryst. Liq. Cryst.* **397**, 347–358.
Jäckel, F., Watson, M. D., Müllen, K. & Rabe, J. P. (2004). *Phys. Rev. Lett.* **92**, 188303.
Josefowicz, J. Y., Maliszewskyj, N. C., Idziak, S. H. J., Heiney, P. A., McCauley Jr, J. P. & Smith III, A. B. (1993). *Science*, **260**, 323–326.
Laursen, B. W., Nørgaard, K., Reitzel, N., Simonsen, J. B., Nielsen, C. B., Als-Nielsen, J., Bjørnholm, T., Sølling, T. I., Nielsen, M. M., Bunk, O., Kjaer, K., Tchebotareva, N., Watson, M. D., Müllen, K. & Piris, J. (2004). *Langmuir*, **20**, 4139–4146.
Lee, J.-H., Choi, S.-M., Pate, B. D., Chisholm, M. H. & Han, Y.-S. (2006). *J. Mater. Chem.* **16**, 2785–2791.
Lee, J.-H., Kim, H.-S., Pate, B. D. & Choi, S.-M. (2006). *Physica B*, **385–386**, 798–800.
Lelj, F., Morelli, G., Ricciard, G., Roviello, A. & Sirigu, A. (1992). *Liq. Cryst.* **12**, 941–960.
O'Neill, M. & Kelly, S. M. (2003). *Adv. Mater.* **15**, 1135–1146.
Pate, B. D., Choi, S.-M., Werner-Zwanziger, U., Baxter, D. V., Zaleski, J. M. & Chisholm, M. H. (2002). *Chem. Mater.* **14**, 1930–1936.
Pisula, W., Menon, A., Stepputat, M., Lieberwirth, I., Kolb, U., Tracz, A., Sirringhaus, H., Pakula, T. & Mullen, K. (2005). *Adv. Mater.* **17**, 684–688.
Samori, P., Yin, X., Tchebotareva, N., Wang, Z., Pakula, T., Jäckel, F., Watson, M. D., Venturini, A., Müllen, K. & Rabe, J. P. (2004). *J. Am. Chem. Soc.* **126**, 3567–3575.
Schmidt-Mende, L., Fechtenkötter, A., Müllen, K., Moons, E., Friend, R. H. & MacKenzie, J. D. (2001). *Science*, **293**, 1119–1122.

Schouten, P. G., Warman, J. M., de Haas, M. P., Fox, M. A. & Pan, H.-L. (1991). *Nature (London)*, **353**, 736–737.
Seguy, I., Destruel, P. & Bock, H. (2000). *Synth. Met.* **111–112**, 15–18.
Shklyarevskiy, I. O., Jonkheijm, P., Stutzmann, N., Wasserberg, D., Wondergem, H. J., Christianen, P. C. M., Schenning, A. P. H. J., de Leeuw, D. M., Tomović, Ž., Wu, J., Müllen, K. & Maan, J. C. (2005). *J. Am. Chem. Soc.* **127**, 16233–16237.
Simmerer, J., Glüsen, B., Paulus, W., Kettner, A., Schuhmacher, P., Adam, D., Etzbach, K. H., Siemensmeyer, K., Wendorff, J. H., Ringsdorf, H. & Haarer, D. (1996). *Adv. Mater.* **8**, 815–819.
Simpson, C. D., Wu, J., Watson, M. D. & Müllen, K. (2004). *J. Mater. Chem.* **14**, 494–504.
Smolenyak, P., Peterson, R., Nebesny, K., Törker, M., O'Brien, D. F. & Armstrong, N. R. (1999). *J. Am. Chem. Soc.* **121**, 8628–8636.
Van De Craats, A. M., Stutzmann, N., Bunk, O., Nielsen, M. M., Watson, M., Müllen, K., Chanzy, H. D., Sirringhaus, H. & Friend, R. H. (2003). *Adv. Mater.* **15**, 495–499.
Van Winkle, D. H. & Clark, N. A. (1982). *Phys. Rev. Lett.* **48**, 1407–1410.
Zimmermann, S., Wendorff, J. H. & Weder, C. (2002). *Chem. Mater.* **14**, 2218–2223.